THE JOURNAL OF BIOLOGICAL CHEMISTRY VOL. 286, NO. 15, pp. 13370–13381, April 15, 2011

New Insights into Cytosolic Glucose Levels during Differentiation of 3T3-L1 Fibroblasts into Adipocytes*

Received for publication, November 5, 2010, and in revised form, February 21, 2011 Published, JBC Papers in Press, February 24, 2011, DOI 10.1074/jbc.M110.200980

Petra Brina Kovacic[‡1], Helena H. Chowdhury[‡§1], Jelena Velebit[‡], Marko Kreft[‡§], Jørgen Jensen[¶], and Robert Zorec[‡§2]

From [‡]Celica, Biomedical Center, Technology Park 24, 1000 Ljubljana, Slovenia, the [§]Laboratory for Neuroendocrinology-Molecular Cell Physiology, Institute of Pathophysiology, Faculty of Medicine, University of Ljubljana, Zaloska 4, 1000 Ljubljana, Slovenia, and the [¶]Department of Physical Performance, Norwegian School of Sport Sciences, 0864 Oslo, Norway

Cytosolic glucose concentration reflects the balance between glucose entry across the plasma membrane and cytosolic glucose utilization. In adipocytes, glucose utilization is considered very rapid, meaning that every glucose molecule entering the cytoplasm is quickly phosphorylated. Thus, the cytosolic free glucose concentration is considered to be negligible; however, it was never measured directly. In the present study, we monitored cytosolic glucose dynamics in 3T3-L1 fibroblasts and adipocytes by expressing a fluorescence resonance energy transfer (FRET)-based glucose nanosensor: fluorescent indicator protein FLIPglu-600μ. Specifically, we monitored cytosolic glucose responses by varying transmembrane glucose concentration gradient. The changes in cytosolic glucose concentration were detected in only 56% of 3T3-L1 fibroblasts and in 14% of 3T3-L1 adipocytes. In adipocytes, the resting cytosolic glucose concentration was reduced in comparison with the one recorded in fibroblasts. Membrane permeabilization increased cytosolic glucose concentration in adipocytes, and glycolytic inhibitor iodoacetate failed to increase cytosolic glucose concentration, indicating low adipocyte permeability for glucose at rest. We also examined the effects of insulin and adrenaline. Insulin significantly increased cytosolic glucose concentration in adipocytes by a factor of 3.6; however, we recorded no effect on delta ratio (ΔR) in fibroblasts. Adrenaline increased cytosolic glucose concentration in fibroblasts but not in adipocytes. However, in adipocytes in insulin-stimulated conditions, glucose clearance was significantly faster following adrenaline addition in comparison with controls ($p < 0.001$). Together, these results demonstrate that during differentiation, adipocytes develop more efficient mechanisms for maintaining low cytosolic glucose concentration, predominantly with reduced membrane permeability for glucose.

Adipocytes utilize glucose to supply energy needs for cellular activities and to promote synthesis and storage of lipids in the cell. Glucose utilization is regulated by the supply of intracellular glucose-6-phosphate. This, in turn, depends on the transport of glucose across the cell membrane and its phosphorylation in the presence of hexokinase and ATP. Adipocytes contain two isoforms of a family of proteins that facilitate transport of glucose across the plasma membrane: GLUT1, the constitutive glucose transporter located mainly at the plasma membrane, and GLUT4, the insulin-sensitive glucose transporter (1, 2). The effect of insulin to increase glucose uptake is exerted by stimulating the translocation of GLUT4 from an intracellular pool to the plasma membrane and thus increasing the permeability of the plasma membrane to glucose (3, 4). However, the accompanying changes in dynamics of intracellular glucose concentration in a single adipocyte are not known as, until recently, it was not possible to measure this parameter directly. To image and quantify changes in cytosolic glucose, Fehr *et al.* (6) constructed a fluorescence resonance energy transfer (FRET)-based glucose nanosensor, specifically expressed in cytosol. Nanosensor consists of a bacterial periplasmic glucose/galactose-binding protein, flanked with two green fluorescent protein variants, cyan (CFP) and yellow fluorescent protein (YFP). This construct undergoes a decrease in YFP/CFP ratio upon substrate binding and has been used successfully to estimate changes in cytosolic free glucose concentration in COS-7, CHO, HEK293, C2C12, and other cell types (5, 6).

Determination of intracellular concentration of free glucose is of particular interest in insulin-sensitive cells (muscle and fat) to study the glucose handling under different conditions. 3T3-L1 fibroblasts are derived from mouse embryonic tissue and differentiate into adipocytes *in vitro*. Although 3T3-L1 adipocytes do not absolutely reflect the situation in primary adipocytes, because they exhibit different biology and physiology during maturation (7, 8) in comparison with primary adipose cells or adipocytes *in vivo*, 3T3-L1 adipocytes are still a useful cell type in metabolic studies due to many advantages (9). During cell differentiation, glucose transport becomes highly sensitive to insulin (10, 11) due to the expression of GLUT4, which is lacking in fibroblasts (12, 13).

Here, 3T3-L1 fibroblasts and adipocytes, expressing the glucose nanosensor FLIPglu-600μ, were used to dynamically monitor intracellular glucose responses to varying external glucose concentrations and insulin. Sympathetic nervous system activity has an important role in the regulation of energy metabolism, including energy expenditure and lipolysis (14). Adrenaline stimulates cAMP production and activation of PKA, which activates glycogen phosphorylase and stimulates glycogen breakdown and accumulation of glucose-6-phosphate (15). In

* This work was supported by Grant P3 310 381 from the Ministry of Higher Education, Sciences and Technology of the Republic of Slovenia, by a grant from the Ministry of Higher Education, Sciences and Technology of the Republic of Slovenia (to P. B. K.), and by European Commission GrowBeta Grant QLG1-CT2001/02233.

[1] Both authors contributed equally to this work.

[2] To whom correspondence should be addressed: Laboratory for Neuroendocrinology-Molecular Cell Physiology, Institute of Pathophysiology, Faculty of Medicine, University of Ljubljana, Zaloska 4, 1000 Ljubljana, Slovenia. Tel.: 386-1-543-7020; Fax: 386-1-543-7021; E-mail: robert.zorec@mf.uni-lj.si.

skeletal muscle, adrenaline-stimulated accumulation of glucose-6-phosphate inhibits hexokinase and free glucose accumulates (16). However, the intracellular glucose concentration after adrenaline action has not been examined yet.

Our results show that during differentiation from 3T3-L1 fibroblasts to adipocytes, the intracellular free glucose concentration decreases. Insulin significantly increased cytosolic glucose in adipocytes but not in fibroblasts. Furthermore, we found that adrenaline increased cytosolic glucose concentration in fibroblasts, but not in adipocytes. Our results provide new insights into the cytosolic glucose levels in 3T3-L1 adipocytes during differentiation.

EXPERIMENTAL PROCEDURES

Chemicals—Dulbecco's modified Eagle's medium (DMEM), calf serum (CS),[3] dexamethasone, isobutylmethylxanthine, HEPES, KCl, D-glucose (throughout the study referred to as glucose), NaH_2PO_4, $NaHCO_3$, Oil Red O, phosphate-buffered saline (PBS), paraformaldehyde, bovine serum albumin (BSA), goat serum, Triton X-100, adrenaline, β-escin, iodoacetate, and 2-deoxyglucose were purchased from Sigma. Sorbitol (D-glucitol) was obtained from Calbiochem. Insulin was purchased from Novo Nordisk (Bagsvaerd, Denmark). NaCl, NaOH, and isopropyl alcohol were obtained from Merck (Darmstadt, Germany). $CaCl_2 \times 6H_2O$ was obtained from Riedel De Haen (Seelze-Hannover, Germany). $MgCl_2$ was purchased from Kemika (Zagreb, Croatia). Anti-β_2-adrenergic receptor and anti-GLUT4 rabbit polyclonal antibodies were obtained from Abcam (Cambridge, UK). Goat anti-rabbit IgG antibody and light antifade kit were purchased from Invitrogen, Molecular Probes.

Cell Culture and Cell Preparation—3T3-L1 fibroblasts were grown in DMEM containing 10% CS, as described previously (17). 3T3-L1 fibroblasts were seeded into tissue culture flasks (25 ml) and allowed to grow to 50–80% confluency to maintain fibroblast phenotype or allowed to grow to absolute confluency for the differentiation procedure, respectively. Differentiation was induced with DMEM containing 10% CS, 0.25 mM dexamethasone, 0.5 mM isobutylmethylxanthine, and 174 nM insulin for 2 days (time 0 to day 2). After that, the medium was replaced with DMEM containing 10% CS and 174 nM insulin for the following 2 days (days 2–4). On day 6, most of the cells were differentiated (judged from their accumulation of lipid droplets) and were transferred to DMEM (with 1000 mg/liter glucose) containing 10% CS. Cells were cultured at 37 °C and 5% CO_2. Experiments were performed 2–6 days after cell preparation. 3T3-L1 cells kept at subconfluent density and not exposed to differentiation medium were termed fibroblasts. After the completed differentiation procedure, 3T3-L1 cells that exhibited lipid droplets in the cytoplasm were termed adipocytes; the subpopulation of cells that was exposed to the differentiation medium and expressed the glucose transporter GLUT4 (data not shown) but had no lipid droplets was termed preadipocytes.

The bath solution for cell imaging consisted of (in mM) 131.8 NaCl, 1.8 $CaCl_2$, 5 KCl, 10 HEPES/NaOH, 0.5 NaH_2PO_4, 5 $NaHCO_3$ (pH 7.2). Glucose and sorbitol were added to this solution at various concentrations. Extracellular solutions with various glucose concentrations were superfused directly over the cells using a gravity-fed eight-way superfusion device with electrically controlled solenoid valves (Warner Instruments, VC-8 valve controller, Hamden, CT). A constant volume of extracellular solution within the recording chamber was maintained using a vacuum pump. Superfusion had a flow rate between 5 and 10 ml/min.

3T3-L1 cells expressing the glucose sensor were permeabilized by using β-escin (100 μM for 20–30 s (5)) to estimate the intracellular glucose level and confirm the activity of the FLIP-glu-600μ sensor. The cell membrane permeabilization was established when application and removal of outside glucose caused almost instantaneous change in YFP/CFP ratio. The bath solution was similar to that used for experimental recordings except for Ca^{2+} being omitted from the milieu, and in some experiments, the bath solution for recordings during cell permeabilization consisted of (in mM) 145 KCl, 2 $MgCl_2$, 10 HEPES/KOH, 10 D-glucose (pH 7.2) to prove no difference in the response between the potassium-based and sodium-based superfusion medium.

Immunocytochemical Staining—To identify the expression of β_2-adrenergic receptors and GLUT4 in 3T3-L1 fibroblasts and adipocytes, the primary rabbit anti-β_2-adrenergic receptor and rabbit anti-GLUT4 antibodies (Abcam) were used and marked with secondary goat anti-rabbit antibody conjugated to fluorescent dye Alexa Fluor 546 (Invitrogen, Molecular Probes). 3T3-L1 cells were washed with PBS, fixed in 4% paraformaldehyde in PBS for 15 min, and then incubated in 0.1% Triton X-100 for 10 min at room temperature. Nonspecific staining was reduced by incubating cells in blocking buffer containing 3% BSA and 10% goat serum in PBS at 37 °C for 1 h. Cells were stained with primary antibody (diluted 1:100 and 1:200) in 3% BSA in PBS at 37 °C for 2 h and secondary antibody (diluted 1:600) in 3% BSA in PBS and incubated for 45 min at 37 °C. Subsequently, they were mounted using the light antifade kit (Invitrogen, Molecular Probes). Fluorescence and transmitted light images of immunostained 3T3-L1 fibroblasts and adipocytes were acquired using a Zeiss LSM 510 confocal microscope through a planapochromatic oil immersion objective ($\times$63, numerical aperture (NA) = 1.4), excited by the 543 nm helium-neon laser line.

Nucleofection—Plasmid DNA (FLIPglu-600μ) was extracted from *Escherichia coli* DH5α and purified using a commercially available protocol, the PureYield plasmid miniprep system (Promega). Plasmid was introduced into 3T3-L1 cells by using the Cell Line Nucleofector kit L (for Nucleofector II, Amaxa). Briefly, after trypsinization and centrifugation of the cell suspension, the pellet (1×10^6 to 5×10^6 cells) was resuspended in 100 μl of supplemented Nucleofector Solution L and mixed with 3–5 μg of plasmid DNA. After nucleofection and centrifugation of the cell suspension, the cell pellet was resuspended in cell culture medium. Cells were seeded onto poly-L-lysine-coated coverslips and incubated in a humidified atmosphere at 37 °C and 5% CO_2.

Fluorescence Microscopy—Imaging was performed 24–48 h after nucleofection using a fluorescence microscope Zeiss

[3] The abbreviations used are: CS, calf serum; IAA, iodoacetate; DOG, 2-deoxyglucose; ANOVA, analysis of variance; ΔR, delta ratio.

Axiovert 135 (Zeiss, Oberkochen, Germany) equipped with a Till photonics system and a CCD camera. Dual emission intensity ratios were recorded using monochromator Polychrome IV (Till Photonics, Gräfeling, Germany) with 436 nm/10 nm excitation and two emission filters (465 nm for CFP and 535 nm for YFP) and neutral density filter (optical density = 0.6). YFP and CFP images were acquired simultaneously using a Dual View image splitter (Optical Insights, Tucson, AZ). For analysis, background light intensity was subtracted from the individual YFP and CFP emission. Images of fluorescent 3T3-L1 cells were acquired through a water immersion objective C-Apochromat (×63, numerical aperture (NA) = 1.2) at intervals of 10 or 20 s. Exposure time was 700 ms.

Determination of Changes in YFP/CFP Ratio and Statistical Analysis—FRET was determined as the YFP/CFP emission intensity ratio. Ratio changes (ΔR) were calculated as the difference between average ratios during superfusion with glucose-free medium and superfusion with glucose medium. Intracellular glucose concentrations at respective extracellular glucose were calculated using Equations 1 and 2. The minimum ΔR (ΔR_{min}) at the complete absence of glucose was measured between two superfusions with glucose-free medium, and the maximum ΔR (ΔR_{max}), at saturation with glucose, was measured after permeabilization with β-escin (100 μM) at 10 mM extracellular glucose.

$$S_{[Glc]extra} = (\Delta R_{[Glc]extra} - \Delta R_{min})/(\Delta R_{max} - \Delta R_{min}) \quad \text{(Eq. 1)}$$

$$[Glc]_{intra} = (K_d \times S_{[Glc]extra})/(1 - S_{[Glc]extra}) \quad \text{(Eq. 2)}$$

where $[Glc]_{extra}$ represents extracellular glucose concentration, $S_{[Glc]extra}$ is the normalized value of ΔR at certain extracellular glucose concentrations, and K_d is the glucose binding affinity of FLIPglu-600μ and was determined *in vitro* to be 0.589 mM (6).

Unless stated otherwise, statistics are in the format of mean ± S.E. Differences between two samples were tested by Student's *t* test. If the normality test failed, we used a Mann-Whitney rank sum test. Differences between three or more samples and data with two independent variables were tested by ANOVA analysis, as indicated, and tested post hoc by the Holm-Sidak method when appropriate. If variances of samples were not equal, we used ANOVA on ranks and tested post hoc by the Dunn's method when appropriate. Regression analysis was carried out by standard techniques (Sigma Plot software; SPSS, Inc., Chicago, IL).

RESULTS

Effect of Extracellular Glucose Concentration on YFP/CFP Ratio in 3T3-L1 Cells—3T3-L1 cells were nucleofected with the low affinity glucose nanosensor FLIPglu-600μ, which was transiently expressed in the cytosol (Fig. 1*A*, *right*). To study and quantify changes in cytosolic glucose due to different concentrations of extracellular glucose supply, the YFP/CFP ratio of the nanosensor was recorded. Fig. 1*B* shows a representative recording of the average YFP/CFP ratio of an entire cell in an adipocyte. The addition of 7.5 mM extracellular glucose induced a decrease in YFP/CFP ratio due to accumulation of free glucose in cytosol. Upon removal of extracellular glucose, the YFP/CFP ratio returned to its original value, indicating utilization

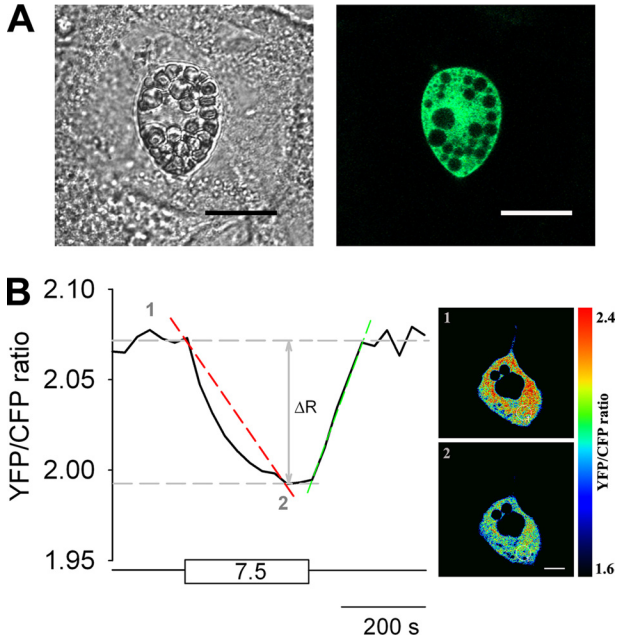

FIGURE 1. **The expression and the activity of glucose nanosensor.** *A*, a transmitted light image (*left*) and a fluorescence image (*right*) of a 3T3-L1 adipocyte transiently expressing the glucose nanosensor FLIPglu-600μ in the cell cytoplasm. *Black spots* on the fluorescent cell image are lipid droplets and cell organelles. *Scale bar*, 20 μm. *B*, diagram showing modulations of the ratio between fluorescence intensities of YFP and CFP in response to changes in external glucose concentration in a single cell. The cell was incubated in extracellular glucose-free medium (*bottom straight horizontal line*), and during superfusion, the cell was supplied with 7.5 mM extracellular glucose (*rectangular box*). The diagram also presents the parameters measured in experiments. The *red dashed line* marks the rate of ratio decline over time (d*R*/d*t*) during the time of superfusion with glucose medium until the steady state in YFP/CFP ratio was reached, as a measure for the rate of glucose load, and the *green dashed line* marks the rate of ratio increase over time (d*R*/d*t*) during the time of superfusion with glucose-free medium until the steady state in ratio was reached, as a measure for the rate of glucose clearance. The *vertical arrow* marks the amplitude (ΔR) of the YFP/CFP ratio change after the addition and removal of glucose from the extracellular solution, respectively (*left panel*). Pseudocolored ratio images (*right panel*) show glucose-dependent YFP/CFP ratio changes. *Red* indicates high ratio or low glucose (*1*, *upper cell image*; 0 mM Glc in extracellular solution), and *blue* indicates low ratio or high glucose (*2*, *lower cell image*; 7.5 mM Glc in extracellular solution). *Scale bar*, 10 μm.

and clearance of cytosolic glucose. During this process, the delta ratio (ΔR) was a measure for changes in cytosolic free glucose concentration. Fig. 1*B*, *right panel*, shows pseudocolored cell images of the YFP/CFP ratio at low (*upper image*) and at high (7.5 mM, *lower image*) extracellular glucose concentrations.

To examine the dynamics of changes in the YFP/CFP ratio due to external glucose supply, cells were superfused with increasing concentrations of extracellular glucose alternating with glucose-free superfusions (Fig. 2). The data of the YFP/CFP ratio changes were compared among three groups of 3T3-L1 cells: fibroblasts, preadipocytes, and adipocytes (see "Experimental Procedures"). The transfection efficiency of FLIPglu-600μ was 6.4% in fibroblasts and 1.4 and 2.5% in preadipocytes and adipocytes, respectively. Interestingly, in many transfected cells, the nanosensor did not respond to alternating extracellular glucose concentrations (Fig. 2*D*). To further study this phenomenon, we counted responsive and unresponsive cells to alternating extracellular glucose concentrations for each of the three cell groups and calculated the corresponding percentages (Table 1). Glucose nanosensor in fibroblasts and

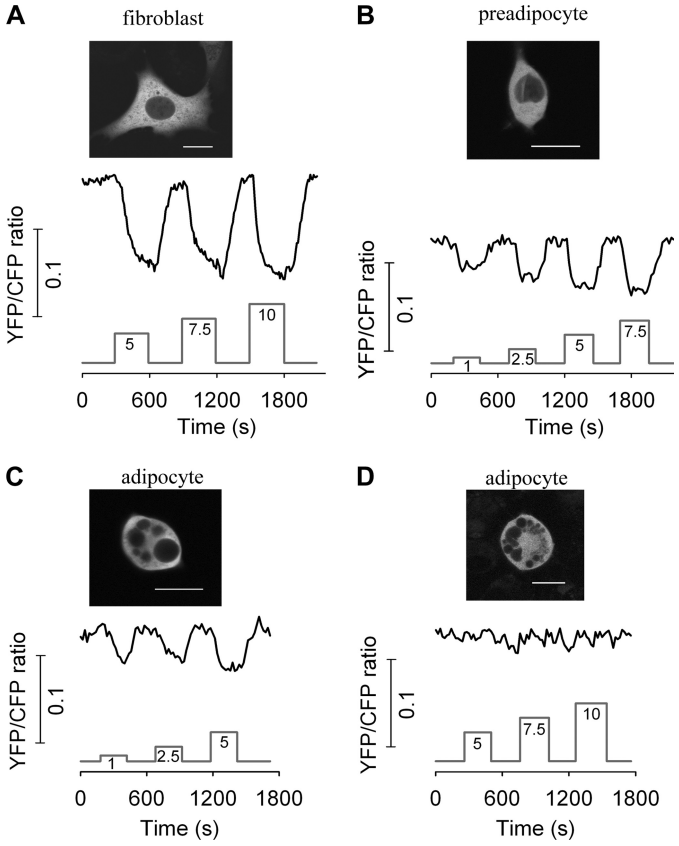

FIGURE 2. **Effect of a stepwise increment of extracellular glucose concentrations on YFP/CFP ratio.** Representative glucose-dependent YFP/CFP ratio changes are shown in a fibroblast (*A*), in a preadipocyte (*B*), and in an adipocyte (*C*). *D*, a representative recording of adipocytes with no response to extracellular glucose (in 86% of cells). Numbers under the *gray step-like traces* indicate the concentration of extracellular glucose (in mM). *Scale bars* on all images: 20 μm.

TABLE 1

Responsiveness (in percentages) to extracellular glucose in three 3T3-L1 cell groups

n represents number of cells examined.

	n	% of responsive cells	% of unresponsive cells
Fibroblasts	32	56.3	43.7
Preadipocytes	109	45.0	55.0
Adipocytes	133	14.3	85.7

preadipocytes responded in about half (56 and 45%, respectively) of cells examined, whereas in adipocytes, the responsiveness was only 14%. In all three cell groups (Fig. 2, *A*–*C*), a stepwise increment of external glucose concentration led to an increasing delta ratio in responsive cells. The maximal average delta ratio of adipocytes (Fig. 2*C*) was lower than in fibroblasts (Fig. 2*A*). In 86% of adipocytes, no YFP/CFP ratio change was observed upon the addition and removal of extracellular glucose (Fig. 2*D*).

Membrane Permeabilization Increases the Responsiveness of 3T3-L1 Cells—To test whether the non-responsive cells express an active glucose nanosensor, we permeabilized the cell membrane of 3T3-L1 cells with β-escin (100 μM) to facilitate glucose entry into the cell (18). After permeabilization of non-responsive cells, the addition and removal of extracellular glucose resulted in an almost instantaneous change in YFP/CFP ratio (Fig. 3*A*), indicating that the lack of response was not due to an inactive glucose nanosensor. In addition, normally responsive cells exhibited an increase in delta ratio after membrane permeabilization in comparison with the delta ratio before membrane permeabilization (Fig. 3*B*). Exposure of fibroblasts to extracellular glucose (10 mM) resulted in the average delta ratio of 0.105 $\pm$ 0.007 ($n = 11$), whereas after membrane permeabilization, the average ΔR increased to 0.125 $\pm$ 0.013 ($n = 6$; Fig. 3*C*, *black columns*) which was, however, not significantly higher. In adipocytes, the average delta ratio at 10 mM extracellular glucose was significantly lower (0.060 $\pm$ 0.008; $n = 8$) when compared with fibroblasts (Fig. 3*C*, $p < 0.01$, two-way ANOVA). However, after membrane permeabilization with β-escin, the delta ratio in adipocytes increased significantly to 0.118 $\pm$ 0.007 ($n = 9$; $p < 0.001$, Fig. 3*C*, *white columns*). Comparisons of the rates of the YFP/CFP ratio changes after application of β-escin show no significant differences in the rate of glucose load (dR/dt) between adipocytes and fibroblasts (data not shown). To verify the activity of nanosensor in the cytosolic, potassium-rich environment, we used a potassium-based superfusion medium during the cell permeabilization with β-escin. The results were similar (data not shown) to that in which the sodium-based medium was used, confirming that under both conditions, the nanosensor was operational.

To further test whether the activity of hexokinase significantly contributes to the non-responsiveness of adipocytes, we treated cells with the glycolytic inhibitor iodoacetate (IAA). IAA selectively blocks the glycolytic enzyme glyceraldehyde-3-phosphate dehydrogenase, which leads to accumulation of glucose-6-phosphate and thus inhibition of hexokinase. After prolonged exposure of non-responsive cells to IAA (100 μM), cells still did not respond to increased extracellular glucose concentration ($n = 4$, Fig. 3*C*).

Differentiation State-dependent Response of 3T3-L1 Cells to External Glucose Supply—We plotted the delta ratios obtained at different external glucose concentrations; the curves were determined by non-linear regression (Fig. 4*A*). In all three cell groups, delta ratios increased with increasing extracellular glucose concentration until saturation was reached above 5 mM external glucose. Statistical analysis (one-way ANOVA) showed that delta ratios obtained upon the addition of extracellular glucose in adipocytes (Fig. 4*A*, *filled triangles*) are significantly smaller when compared with both fibroblasts (Fig. 4*A*, *filled symbols*) and preadipocytes (Fig. 4*A*, *filled squares*) at a concentration of 5 mM ($p < 0.001$) and when compared with fibroblasts at a concentration of 10 mM ($p < 0.05$), respectively. There were no significant differences between delta ratios of fibroblasts and preadipocytes. At 5 mM extracellular glucose, insulin was applied to fibroblasts and to adipocytes, respectively. Although there was no particular effect of insulin on ΔR (0.111 $\pm$ 0.005 before and 0.113 $\pm$ 0.005 after insulin stimulation) in fibroblasts (Fig. 4*A*, *gray circle*), there was, however, a significantly higher ΔR obtained after insulin stimulation (0.088 $\pm$ 0.017) in adipocytes (Fig. 4*A*, *gray triangle*) when compared with non-stimulated conditions (0.055 $\pm$ 0.005; $p <$ 0.05). In Fig. 4*A*, *open symbols* denote delta ratio in cells with no apparent response to extracellular glucose. To estimate the intracellular glucose concentrations at different extracellular

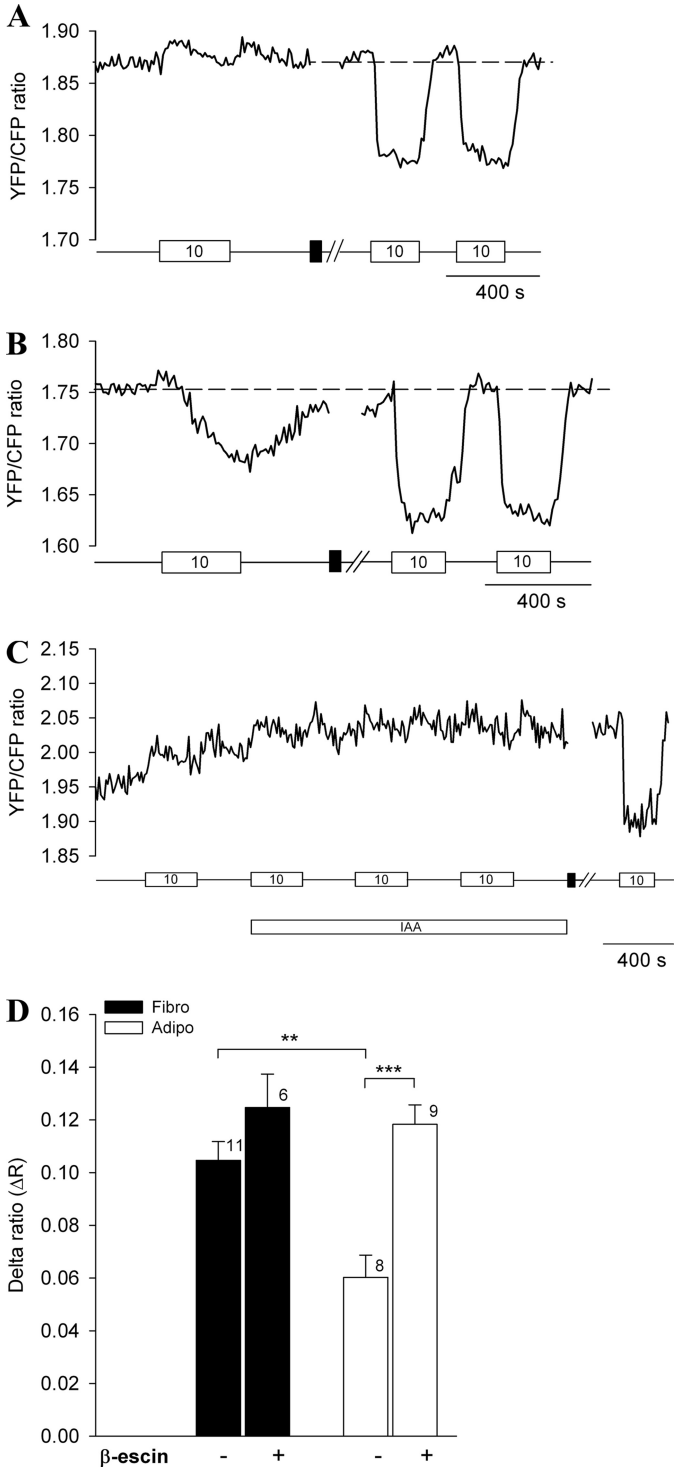

FIGURE 3. **Intracellular glucose levels increased in cells permeabilized with β-escin.** *A*, the initial part of the recording shows a representative recording of the YFP/CFP ratio in a 3T3-L1 adipocyte devoid of response to the exposure to 10 mM extracellular glucose concentration. However, the application of 100 μM β-escin (*black box*) for 20–30 s caused the nanosensor to respond reversibly to the 10 mM extracellular glucose pulses (*rectangular boxes*), indicating the normal function of the FLIPglu-600μ sensor. The application of β-escin caused an artifact, which was not displayed (//). *B*, representative recording of the YFP/CFP ratio in a 3T3-L1 adipocyte that normally responded to the addition of extracellular glucose before the β-escin application. However, after the membrane permeabilization, the delta ratio significantly increased. *C*, representative recording of the YFP/CFP ratio changes in 3T3-L1 adipocyte unresponsive to 10 mM extracellular glucose concentration. The exposure of cell to iodoacetate (100 μM), an inhibitor of glycolysis, failed to provoke a response to extracellular glucose. Subsequent application of β-escin caused the nanosensor to respond reversibly to the 10 mM extracellular glucose pulse. *D*, histogram shows delta ratio during changes in extracellular glucose from 0 to 10 mM in fibroblasts (*black columns*) and in adipocytes (*white columns*) before and after permeabilization with β-escin. *Numbers* above columns indicate numbers of cells tested; *error bars* show S.E. *Asterisks* indicate significant differences (**, $p < 0.01$ and ***, $p < 0.001$, two-way ANOVA).

glucose supply, we used Equations 1 and 2. ΔR_{min} was measured during two superfusions with glucose-free medium, ΔR_{max} was determined as the average ΔR obtained after permeabilization with β-escin, and K_d is 0.589 μM as measured *in vitro* (6). Results are summarized in Fig. 4*B*. Cytosolic glucose levels increased with increasing extracellular glucose. In fibroblasts, the cytosolic glucose concentration yielded values up to 5 mM, and in preadipocytes, the cytosolic glucose concentration yielded values up to 2.5 mM; however in adipocytes, cytosolic glucose did not exceed 1 mM. Fitting the one-site saturation ligand binding curve to the data of cytosolic glucose concentrations yielded the predicted maximal values of cytosolic glucose concentration (Fig. 4*B*, *dashed lines*): 10.23 mM for fibroblasts, 2.63 mM for preadipocytes, and 0.58 mM for adipocytes. In insulin-stimulated adipocytes (*gray triangle*), cytosolic glucose concentration (1.57 mM) increased by a factor of ~4 when compared with non-stimulated adipocytes (0.44 mM), whereas in fibroblasts, the cytosolic glucose concentration did not increase significantly after insulin stimulation. Rates of glucose load and clearance were calculated as derivatives of the YFP/CFP ratio over time (dR/dt). The rate of glucose load was calculated from the time of glucose addition in extracellular solution to the time when the ratio reached a steady state (Fig. 1*B*, *red dashed line*), and the rate of glucose clearance was calculated from the beginning of superfusion with glucose-free medium to the time when the ratio reached a steady state (Fig. 1*B*, *green dashed line*). Results are summarized in Fig. 4*C*. We compared the rates between different external glucose supplies (one-way ANOVA). In fibroblasts (*black bars*), there was a significantly smaller rate of glucose load measured at 1 mM glucose when compared with 2.5 and 5 mM glucose concentrations ($p < 0.01$). In preadipocytes (*gray bars*) and in adipocytes (*white bars*), there were no significant differences in glucose load at different external glucose concentrations. We then compared the rates of glucose load between all three cell groups. Statistical comparison shows a significantly slower rate of glucose load in adipocytes when compared with preadipocytes at external glucose concentrations of 5 mM ($p < 0.05$). There were no significant differences between basal and insulin-stimulated (data not shown) rates of glucose load. Fig. 4*C*, *right panel*, summarizes the rates of glucose clearance, which were normalized to the glucose concentration gradient across the plasma membrane; we have taken into account the measured values of cytosolic glucose concentrations in Fig. 4*B* at particular extracellular glucose levels. In fibroblasts, the rate of glucose clearance decreased with increasing glucose concentration gradient across the plasma membrane ($p < 0.001$ for 1 mM *versus* all higher concentrations). Preadipocytes show a significantly higher glucose clearance rate ($p < 0.01$) at 1 mM when compared with 5, 7.5, and 10 mM external glucose concentrations,

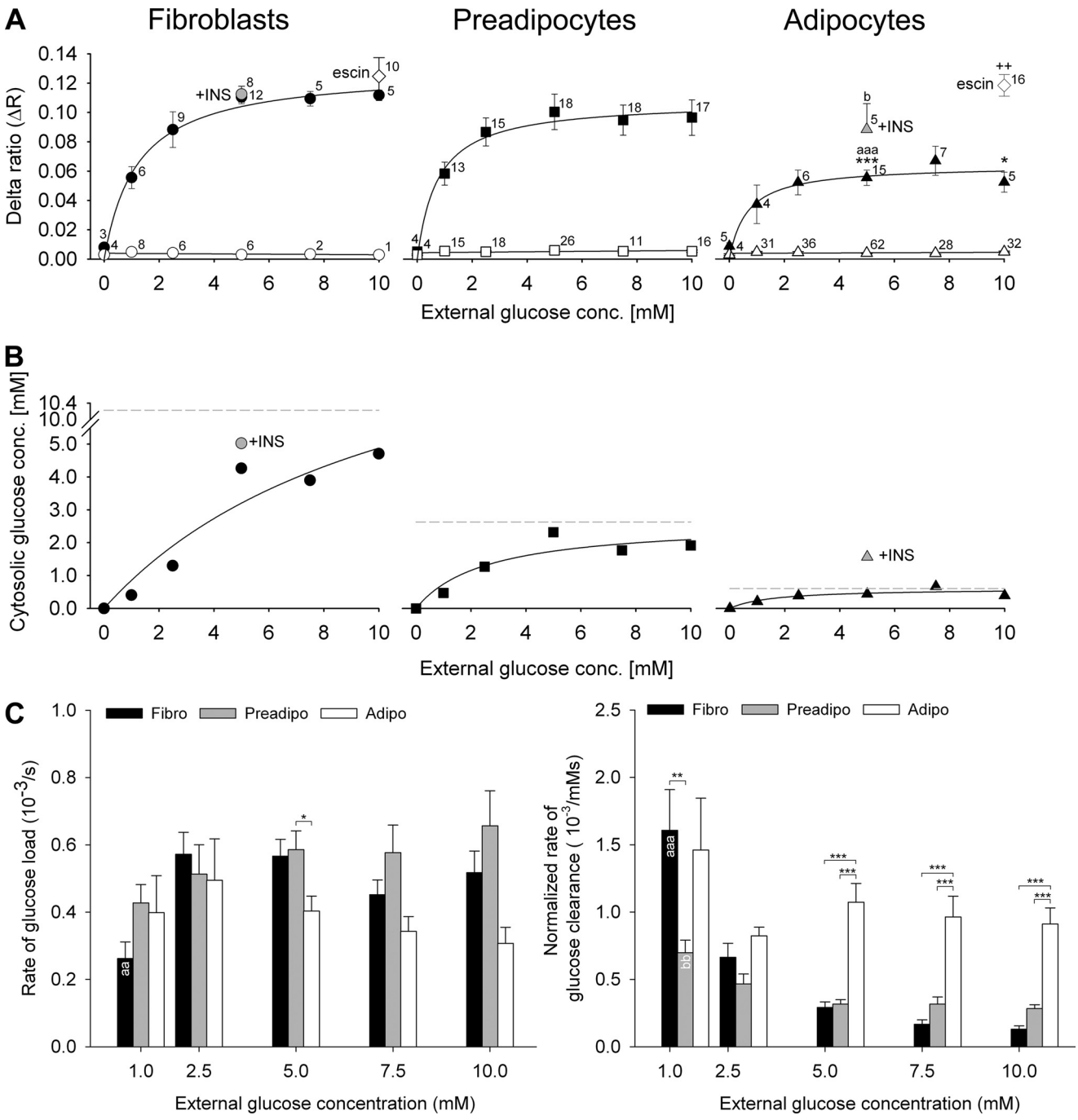

FIGURE 4. **Determination of cytosolic glucose concentration at different external glucose levels.** *A*, extracellular glucose-dependent mean ΔR of 3T3-L1 fibroblasts, preadipocytes, and adipocytes. Delta ratios were calculated as the difference between the average YFP/CFP ratios during superfusion with and without glucose in the superfusion medium. The *numbers* adjacent to the symbols indicate the numbers of measurements for explicit extracellular glucose concentrations (*conc.*) obtained from responsive (*filled symbols*) and unresponsive (*open symbols*) cells to alternating extracellular glucose concentration. *Gray symbols* denote insulin (*INS*)-stimulated measurements. *White diamonds* are mean measurements of permeabilized cells with β-escin. Differences in delta ratios were compared: ΔR of adipocytes *versus* ΔR of fibroblasts (*); ΔR of adipocytes *versus* ΔR of preadipocytes (*a*); ΔR of insulin-stimulated *versus* ΔR of non-stimulated conditions (*b*); ΔR of permeabilized *versus* ΔR of non-permeabilized cells (+). Statistical significance is denoted: * and *b*, $p < 0.05$; ++, $p < 0.01$; *aaa* and ***, $p < 0.001$. For statistical comparison of groups, Student's *t* test and ANOVA analysis were employed. The curves represent best fits obtained by non-linear regression and the equation $\Delta r = (\Delta R_{max} \times [Glc]_{extra})/(K_d + [Glc]_{extra})$. *B*, ratio changes were transformed into cytosolic glucose concentrations using Equations 1 and 2. *Gray symbols* denote mean values of cells stimulated with insulin. Note that in insulin-stimulated adipocytes, cytosolic glucose concentration increased by a factor of 3.6 when compared with non-stimulated adipocytes. *Solid lines* are best fits of one-site saturation ligand binding curve. *Dashed gray lines* represent the predicted maximal values of cytosolic glucose concentrations: 10.2 mM in fibroblasts, 2.6 mM in preadipocytes, and 0.6 mM in adipocytes. *C*, rates of glucose load and clearance at different external glucose supply in fibroblasts (*Fibro*, *black bars*), preadipocytes (*Preadipo*, *gray bars*), and adipocytes (*Adipo*, *white bars*). Statistically significant differences between rates of different cell groups at the same external glucose supply are denoted: *, $p < 0.05$; **, $p < 0.01$; ***, $p < 0.001$. The rate of glucose load in fibroblasts at 1 mM extracellular glucose is significantly slower from all higher concentrations of glucose supply (*aa*). The rate of glucose clearance in fibroblasts at 1 mM is significantly slower when compared with rates at all higher external glucose concentrations (*aaa*), and the rate of glucose load in preadipocytes at 1 mM is significantly slower when compared with rates at 5, 7.5, and 10 mM external glucose concentrations (*bb*).

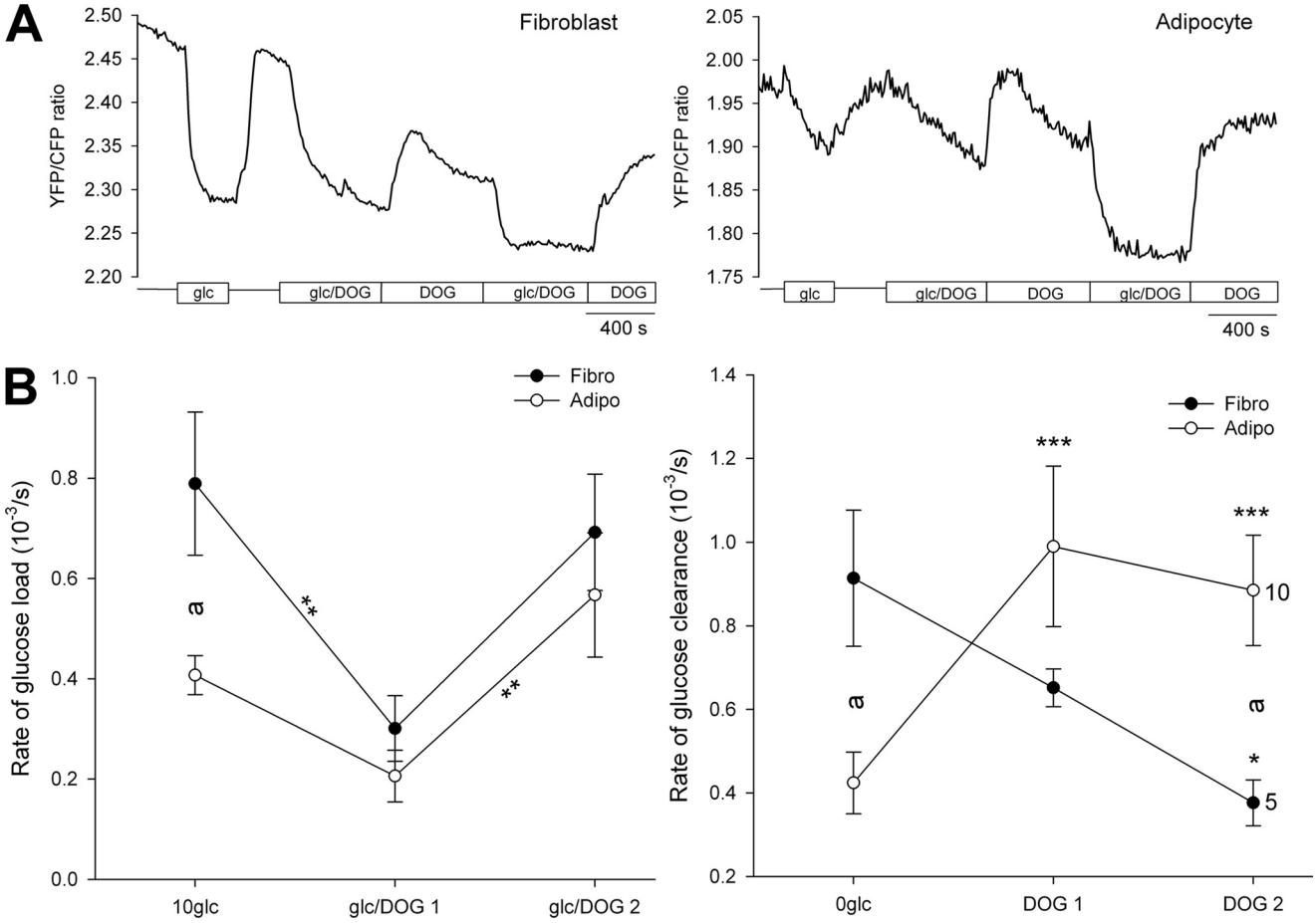

FIGURE 5. **Intracellular glucose levels in the presence of 2-deoxyglucose.** *A*, representative recordings of the YFP/CFP ratio in a 3T3-L1 fibroblast (*left panel*) and a 3T3-L1 adipocyte (*right panel*) superfused with DOG (30 mM) in the presence or absence of 10 mM extracellular glucose (*rectangular boxes*). *B*, the effect of DOG on the rate of glucose load (*left panel*) after the addition of extracellular glucose (10 mM) and clearance (*right panel*) obtained after superfusion with glucose-free extracellular solution in fibroblasts (*black dots*) and in adipocytes (*white dots*), measured as d*R*/d*t*. The *numbers* adjacent to the symbols indicate the numbers of cells tested; *error bars* show S.E. Significant differences are denoted: *a* and *, $p < 0.01$; **, $p < 0.01$; ***, $p < 0.001$, two-way RM ANOVA.

respectively. Adipocytes show no significant differences of glucose clearance rate at different external glucose supply. Comparison of the glucose clearance rates between all three cell groups revealed a significantly higher rate in fibroblasts when compared with preadipocytes ($p < 0.05$) at 1 mM extracellular glucose concentration. Adipocytes show a significantly higher rate of glucose clearance when compared with fibroblasts and preadipocytes at 5, 7.5, and 10 mM extracellular glucose concentrations ($p < 0.001$). These results are consistent with the view that the rate of glucose load is slower in adipocytes than in fibroblasts and that the rate of normalized glucose clearance is higher in adipocytes than in fibroblasts.

Glucose Dynamics in the Presence of 2-Deoxyglucose—The glucose analog 2-deoxyglucose (DOG) is widely used in glucose metabolic studies as it inhibits hexokinase by the accumulation of 2-deoxyglucose phosphate (19, 20) and thus acts as an inhibitor of glucose metabolism and also as a competitive inhibitor for glucose transport. The glucose nanosensor FLIPglu-600μ is insensitive to DOG concentrations of ~10–30 mM, which is lower than the reported sensitivity of the FLIPglu-600μ at >100 mM (5, 6). We superfused cells with DOG in the absence and presence of 10 mM glucose (Fig. 5*A*). The rate of glucose load during the first glucose/DOG superfusion was reduced in both cell groups, likely due to competition between glucose and DOG for glucose transporters (Fig. 5*B*). In fibroblasts, the rate of glucose load was significantly reduced (in 10^{-3} arbitrary units/s) from 0.79 ± 0.14 to 0.30 ± 0.07 ($p < 0.01$; two-way RM ANOVA), whereas in adipocytes, the reduction was not significant, from 0.41 ± 0.04 to 0.21 ± 0.05 (Fig. 5*B*, *left panel*). During the second glucose/DOG superfusion, the glucose load rate increased in fibroblasts (0.69 ± 0.12), as well as in adipocytes (0.57 ± 0.12, $p < 0.01$, when compared with glucose load rate during the first glucose/DOG superfusion). This indicates that although the glucose influx is partially inhibited due to the competition with DOG, glucose phosphorylation is even more reduced, probably due to the inhibition of hexokinase; therefore, free glucose accumulates. This is also supported by lower YFP/CFP ratio in both cell groups (Fig. 5*A*). After first and second washout of glucose from extracellular medium with superfusion in the presence of DOG, in fibroblasts (Fig. 5*B*, *right panel*), the rate of glucose clearance gradually decreased (0.65 ± 0.05 and 0.38 ± 0.05; $p < 0.05$) when compared with the rate of clearance in the absence of DOG (0.91 ± 0.16). This result is consistent with hexokinase inhibition by DOG (19, 20). In adipocytes, the rate of glucose clearance significantly increased after the first (0.99 ± 0.19; $p < 0.001$) and also after

the second (0.89 ± 0.13) washout of glucose when compared with the rate in the absence of DOG (0.54 ± 0.12; Fig. 5*B*, *right panel*). Experiments were performed on 5 fibroblasts and 10 adipocytes, and data were analyzed with two-way RM ANOVA.

Effect of Insulin and Adrenaline on YFP/CFP Ratio in Fibroblasts and Adipocytes—To study the effect of insulin on the YFP/CFP ratio, cells were superfused alternately with high glucose (5 mM) and glucose-free medium, and during these alternations, insulin was added to reach a final concentration of 100 nM (Fig. 6, *A* and *B*). Consistent with experiments shown in Table 1 and Fig. 4, there was again a high percentage of cells (33% of fibroblasts and 93% of adipocytes) where no response was detected to alternating extracellular glucose concentrations, and also, none of these cells responded after insulin application (data not shown). In responsive fibroblasts (Fig. 6*A*), insulin caused a small, but not statistically significant, decrease in the delta ratio. Importantly, in responsive adipocytes, insulin stimulation at high glucose concentrations resulted in a significantly increased ($p < 0.01$) delta ratio when compared with the delta ratio recorded prior to the application of insulin (Fig. 6*B*). This result is consistent with the view that insulin augments the permeability for glucose entry into adipocytes.

The effect of adrenaline on basal and insulin-stimulated YFP/CFP ratio changes was examined. The presence of β-adrenergic receptors in fibroblasts and in adipocytes was confirmed by immunocytochemical labeling (data not shown). Cells were superfused with extracellular solution containing alternating glucose concentrations without (Fig. 6, *C* and *D*) or with 100 nM insulin (Fig. 6, *E* and *F*). During the experiment, adrenaline was added into the superfusion solution to reach a final concentration of 1 μM. In basal conditions, adrenaline increased ΔR in both cell groups, whereas in insulin-stimulated conditions, adrenaline did not cause any significant change in the delta ratio (Fig. 6, *E* and *F*).

Statistical analyses of delta ratios of responsive cells due to glucose entry after insulin and adrenaline stimulation, respectively, are summarized in Fig. 6*G* (two-way RM ANOVA). In fibroblasts, the average ΔR at 5 mM external glucose was 0.12 ± 0.01; after insulin action, ΔR did not change significantly and was 0.11 ± 0.01 ($n = 8$). Adipocytes responded to 5 mM glucose with ΔR of 0.06 ± 0.01. Insulin stimulation caused a significant increase in ΔR to a value of 0.09 ± 0.02 ($n = 5$; $p < 0.01$), consistent with data in Fig. 4 (non-paired) and the view that insulin enhances the permeability of the plasma membrane for glucose in adipocytes. In cells stimulated with adrenaline, there was an increased cytosolic glucose concentration. In fibroblasts, ΔR increased from 0.09 ± 0.02 to 0.12 ± 0.02 ($n = 7$), which is statistically significant ($p < 0.05$). Adipocytes responded to 5 mM extracellular glucose after adrenaline application with ΔR of 0.07 ± 0.01, which was higher but not significantly different from ΔR before adrenaline application (0.06 ± 0.01). Adrenaline application had no significant effects on cytosolic glucose dynamics in insulin-stimulated 3T3-L1 cells; in fibroblasts, the ΔR decreased from 0.12 ± 0.01 to a 0.11 ± 0.01 ($n = 7$), whereas in adipocytes, ΔR slightly increased after adrenaline application from 0.068 ± 0.003 to 0.074 ± 0.004 ($n = 7$).

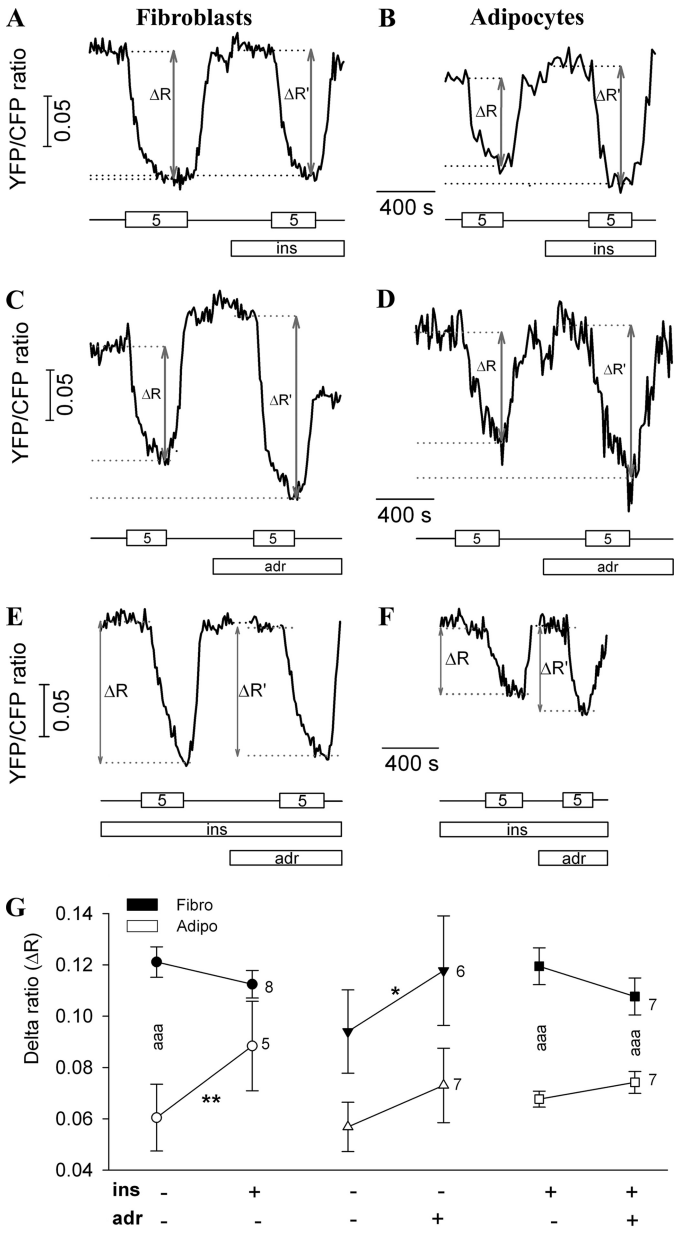

FIGURE 6. **Effects of insulin and adrenaline on ΔR.** *A* and *B*, the graphs show a real time recording of the YFP/CFP ratio during the superfusion with alternating glucose concentrations (0 and 5 mM). Insulin (100 nM) was present in extracellular medium during the second half of the experiment (*lower bar*). *Gray arrows* represent the delta ratio before (Δ*R*) and after (Δ*R'*) the addition of insulin. The *numbers* in the *boxes* indicate the concentration of extracellular glucose (in mM), and the *lines* between the *boxes* indicate the glucose-free solution. *C* and *D*, the graphs show YFP/CFP ratio recordings in a fibroblast (*C*) and in an adipocyte (*D*) during the superfusion with alternating glucose concentrations (0 and 5 mM) before and after adrenaline application. *ins*, insulin. *E* and *F*, representative recordings of the effect of adrenaline on insulin-stimulated YFP/CFP ratio change in fibroblast (*E*) and adipocyte (*F*). Insulin (100 nM) was present in the extracellular solution from the start of the recording (*ins, middle bar*), whereas adrenaline (*adr*, 1 μM) was added in the second part of the experiment (*lower bar*). *Gray arrows* represent delta ratio before (Δ*R*) and after (Δ*R'*) the addition of 1 μM adrenaline. *G*, scatter-line plot shows ΔR before and after insulin addition (*left*), adrenaline addition (*middle*), and adrenaline addition in insulin-stimulated cells (*right*) in fibroblasts (*Fibro*, *black symbols*) and in adipocytes (*Adipo*, *white symbols*). *Numbers* adjacent to symbols indicate number of cells tested; *error bars* show S.E. *Asterisks* indicate significant differences (*, $p < 0.05$; **, $p < 0.01$; aaa, ***, $p < 0.001$; two-way RM ANOVA).

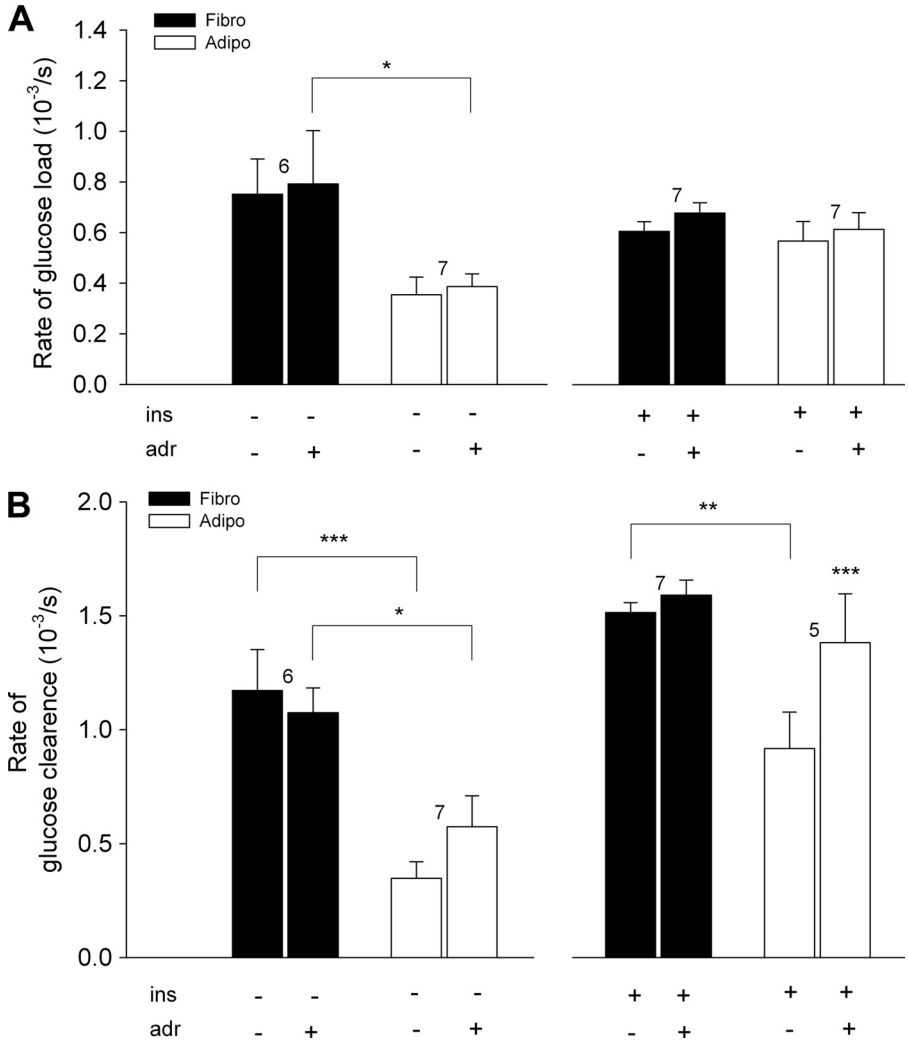

FIGURE 7. **The effect of adrenaline (*adr*, 1 μM) application on the rate of glucose load and clearance measured as d*R*/dt.** *A*, the rate of glucose load obtained after the addition of extracellular glucose (5 mM) in fibroblasts (*Fibro*, *black columns*) and in adipocytes (*Adipo*, *white columns*) in basal (*left panel*) and insulin-stimulated (*ins*, 100 nM, *right panel*) conditions. *B*, the rate of glucose clearance obtained after superfusion with glucose-free extracellular solution in fibroblasts (*black columns*) and in adipocytes (*white columns*) in basal (*left panel*) and insulin-stimulated (100 nM, *right panel*) conditions. *Numbers* above columns indicate the number of cells tested; *error bars* show S.E. *Asterisks* indicate significant difference (*, $p < 0.05$; **, $p < 0.01$; ***, $p < 0.001$; two-way RM ANOVA).

To further study the effect of adrenaline on intracellular glucose dynamics, we measured the rate of the YFP/CFP ratio change. The rates of glucose load and clearance were measured as the derivative of the YFP/CFP ratio change over time (dR/dt) (see results in Fig. 4*C* and the legend for Fig. 1*B*). The average rates of the YFP/CFP ratio changes during insulin or adrenaline stimulation are shown in Fig. 7. In basal conditions, the rate of glucose load (in 10^{-3}/s) after adrenaline addition did not change significantly (Fig. 7*A*) in fibroblasts (from 0.75 ± 0.14 to 0.79 ± 0.21; $n = 6$) or in adipocytes (from 0.35 ± 0.07 to 0.39 ± 0.05; $n = 7$). Similar changes were observed in insulin-stimulated conditions; the rate of glucose load after adrenaline addition slightly increased in fibroblasts from 0.61 ± 0.04 to 0.68 ± 0.04 ($n = 7$) and also in adipocytes from 0.57 ± 0.08 to 0.61 ± 0.07 ($n = 7$). In insulin-stimulated conditions, the rate of glucose load in adipocytes reached that in fibroblasts. The rate of the YFP/CFP ratio increase due to washout of external glucose (Fig. 7*B*) did not change significantly after adrenaline addition in basal conditions (from 1.17 ± 0.18 to 1.08 ± 0.11 in fibroblasts, $n = 6$, and from 0.35 ± 0.08 to 0.57 ± 0.14 in adipocytes, $n = 7$), but the overall clearance rate was significantly slower in adipocytes when compared with fibroblasts (Fig. 7*B*, *left panel*). In insulin-stimulated conditions (Fig. 7*B*, *right panel*), the rate of glucose clearance after adrenaline addition did not change in fibroblasts (from 1.51 ± 0.04 to 1.59 ± 0.07; $n = 7$). However, in adipocytes, it increased significantly ($p < 0.001$) with adrenaline stimulation to 1.38 ± 0.21 when compared with 0.92 ± 0.16 ($n = 5$). In adipocytes, the rate of glucose clearance was lower than in fibroblasts only before the adrenaline addition ($p < 0.01$). All statistics were analyzed with two-way RM ANOVA.

DISCUSSION

We investigated the dynamics of intracellular glucose concentration in single 3T3-L1 cells. We used a FRET-based glucose nanosensor FLIPglu-600μ, which undergoes a decrease in YFP/CFP ratio upon binding of glucose and is insensitive to phosphorylated glucose or glycolytic intermediates (6). Intracellular glucose concentration reflects the balance of glucose

entry across the plasma membrane and glucose phosphorylation. Biochemical analysis of intracellular concentration of free glucose in intact tissue is difficult because correction of extracellular glucose is hard to do accurately. Here, we examined the effect of alternating extracellular glucose concentration on YFP/CFP ratio and the effects of insulin and adrenaline on intracellular glucose dynamics.

The Effect of Alternating Extracellular Glucose Concentration on YFP/CFP Ratio and on Cytosolic Glucose Concentration—3T3-L1 cells were transfected with DNA construct encoding FLIPglu-600μ glucose nanosensor, which was expressed in the cytosol (Fig. 1*A*). After exposing cells to high glucose, the YFP/CFP ratio dropped, indicating an elevated concentration in cytosolic glucose (Fig. 1*B*). Removal of extracellular glucose led the YFP/CFP ratio to return to a starting value, demonstrating the reversibility of glucose binding to the nanosensor (Fig. 1*B*), as reported for other cell types (6).

We compared YFP/CFP ratio changes due to different concentrations of externally supplied glucose among three groups of cells: fibroblasts, preadipocytes, and adipocytes (see "Experimental Procedures"). Ratio changes (ΔR) were calculated as the difference between average ratios during superfusion with glucose-free medium and superfusion with glucose medium. A stepwise increment of external glucose concentrations led to an increase of delta ratio in all three cell groups (Fig. 2, *A*–*C*). The surprising observation was that in many cells, especially adipocytes, external glucose did not cause a change in YFP/CFP ratio (Fig. 2*D*).

From all cells tested (Table 1), we found that a major portion of adipocytes (86%) did not respond to external glucose; among fibroblasts and preadipocytes, 45 and 56% of cells were unresponsive, respectively. It is unlikely that the unresponsiveness is due to an inactive sensor because membrane permeabilization with β-escin (5) restored the responsiveness (Fig. 3*A*). We cannot exclude the possibility that in unresponsive cells, the glucose uptake is reduced to such an extent that the glucose utilization equals glucose uptake, and therefore, no free glucose is available to be detected by the nanosensor. Therefore, it is likely that in non-responsive cells, mechanisms responsible for glucose handling prevent any free glucose from appearing in the cytosol.

Membrane permeabilization by β-escin in cells that responded to altering extracellular glucose concentration resulted in an increase in the response. This indicates that cytosolic free glucose concentration considerably depends on the membrane permeability for glucose (Fig. 3*B*). Treatment with β-escin resulted in an increased delta ratio in fibroblasts and in adipocytes. However, in fibroblasts, this difference was not significant (Fig. 3*C*, *left columns*), whereas in adipocytes, there was a statistically significant increase in the delta ratio after permeabilization with β-escin (Fig. 3, *B* and *C*, *right columns*), reaching the value recorded in fibroblasts. This result suggests that the membrane permeability of adipocytes is relatively lower in comparison with that in fibroblasts. Consequently, the free glucose that enters the cell is rapidly phosphorylated by hexokinase, and therefore, its concentration is low or even below the level of detection by FLIPglu-600μ ($\sim$70 μM). These results are also consistent with recent findings (5) that the rate of glucose uptake has a profound effect on the level of intracellular free glucose.

In all three cell groups, the delta ratio was increasing until the saturation reached above $\sim$5 mM external glucose (Fig. 4*A*). In adipocytes, the average delta ratios at 5 mM extracellular glucose were significantly smaller when compared with both fibroblasts and preadipocytes (Fig. 4*A*). We estimated the cytosolic glucose concentration by using the K_d determined *in vitro* (6) and ΔR_{max} measured after membrane permeabilization in calculations. Results indicate that there is a lower concentration of free glucose in adipocytes when compared with fibroblasts or compared with preadipocytes in the same extracellular glucose environment, which can be explained by at least two simultaneous mechanisms. 1) Adipocytes have a relatively diminished resting membrane permeability for glucose, which leads to a lower influx of glucose into the cell and therefore to a smaller ratio change after binding to nanosensor. 2) The metabolism in adipocytes may be very efficient in glucose utilization, and therefore, glucose that enters into the cytosol is rapidly phosphorylated, and therefore, not detected by the nanosensor. The gradually smaller cytosolic free glucose concentration from fibroblasts to adipocytes could be explained by the maturing of glucose-handling machinery in the direction of maintaining low cytosolic glucose concentration, which includes increased glycogen synthesis and glucose metabolism and decreased membrane permeability for glucose. It has been already reported that GLUT1 on the surface of 3T3-L1 adipocytes has attenuated intrinsic activity when compared with GLUT1 of fibroblasts (21). Due to differences in the expression of glucose transporters (1, 2, 12, 13, 23), the fibroblast membrane is constitutively relatively more permeable for glucose, whereas the plasma membrane of adipocytes becomes more glucose-permeable only after insulin action and translocation of GLUT4 to the plasma membrane, which we demonstrated by the 3.6-fold increase in cytosolic glucose concentration (Fig. 4*B*). The lower glucose load rate in adipocytes when compared with both fibroblasts and preadipocytes at high (5 mM and above) external glucose concentrations (Fig. 4*C*) also supports the notion of a relatively lower membrane permeability for glucose in adipocytes *versus* fibroblasts. Furthermore, results obtained with the glycolytic inhibitor (22) IAA show that even after prolonged exposure of non-responsive adipocytes to IAA, glucose does not accumulate in cells (Fig. 3*C*). This result suggests that either IAA does not adequately inhibit glycolysis (which is possible but less likely) or membrane permeability for glucose is low. On the other hand, very efficient metabolism in adipocytes is supported by the significantly higher rate of glucose clearance in adipocytes when compared with fibroblasts and preadipocytes (Fig. 4*C*, *right panel*). Results with DOG show a significantly higher rate of glucose load after second treatment with Glc/DOG (Fig. 5*B*), indicating that glycolysis was inhibited in both fibroblasts and adipocytes. In fibroblasts, a gradually decreased rate of glucose clearance after inhibition of glycolysis by DOG also supports this. In adipocytes, however, the rate of glucose clearance in the presence of DOG was significantly increased, which cannot be explained by the inhibition of glycolysis; thus, the mechanism remains to be studied in the future. Still, after 10

min with DOG, intracellular glucose increased as expected when external glucose was added (Fig. 5*A*).

The Effect of Insulin and Adrenaline on Cytosolic Glucose Concentration—Insulin plays an important role in adipocytes, not only for glucose permeability but also in metabolism of these cells (24–27). Although the concept of glucose-induced insulin resistance is well documented, the underlying mechanisms are still not well understood.

We examined the effect of insulin on cytosol glucose dynamics. Fibroblasts responded to insulin with no significant change in the cytosolic glucose concentration (Figs. 4*B* and 6*A*). Adipocytes responded with a significant increase in the delta ratio (~50%) following the insulin addition (Fig. 6*B*), resulting in 3.6-fold increase in cytosolic glucose concentration, which reached 1.6 mM (Fig. 4*B*). These results are consistent with an increase in cytosolic glucose due to insulin-facilitated glucose transport across the cell membrane by GLUT4 in adipocytes (10, 11). However, the novel aspect obtained by these experiments is that the value of 1.6 mM intracellular free glucose is considerably below the glucose concentration measured in fibroblasts (4.3 mM) at the same extracellular glucose environment. Considering the fact of increased glucose permeability in insulin-stimulated adipocytes, these data support the idea that glucose utilization in adipocytes becomes even more efficient after insulin action. In skeletal muscle, insulin does not increase the intracellular concentration of free glucose (16) unless the extracellular concentration of glucose is high (28). These data indicate that in the flux through the glycolytic pathway, glucose transport is slower than the activity of hexokinase in 3T3-L1 cells in basal and in insulin-stimulated conditions. The fact that some, but not all, cells responded with elevated concentration of free glucose shows that 3T3-L1 adipocytes are a heterogeneous population, which is not observed in biochemical analysis.

3T3-L1 adipocytes express three subtypes of β-adrenergic receptors (29), and the β_3-adrenergic receptor has been found to be dramatically increased (30) after differentiation. Several mechanisms have been proposed by which β-adrenergic receptor stimulation may affect insulin-stimulated glucose uptake in 3T3-L1 and rat adipocytes (12, 31–34).

To investigate how adrenergic receptor stimulation affects YFP/CFP ratio changes, we treated basal and insulin-stimulated cells with 1 μM adrenaline. In basal conditions, adrenaline caused a significant increase in ΔR only in fibroblasts (Fig. 6, *C* and *G*, *middle plot*; $p < 0.05$); however, in insulin-stimulated conditions, adrenaline had no significant effect on cytosolic glucose concentration in 3T3-L1 cells (Fig. 6*G*, *right plot*). It has been shown that insulin-stimulated glucose uptake in rat and 3T3-L1 adipocytes could be reduced upon treatment with adrenaline, nor-adrenaline, and isoproterenol (33–36). Some studies report that β-adrenergic receptor agonists attenuate insulin-stimulated glucose uptake by decreasing the translocation of GLUT4 in rat and 3T3-L1 adipocytes (31, 34). Other studies (37) report that the binding of insulin to its receptor is attenuated, which probably results in a less stimulatory signal and, as a consequence, in a reduced increase in the rate of glucose uptake. Our data on 3T3-L1 cells also contrast the data from skeletal muscle in which adrenaline causes accumulation of free glucose because glucose-6-phopsphate accumulation inhibits hexokinase, whereas insulin-stimulated glucose transport is not reduced (16). Therefore, it is possible that the lack of change in cytosolic free glucose concentration after adrenaline application in adipocytes could be the result of adrenaline-inhibited glucose influx accompanied by an inhibition of hexokinase by stimulation of glycogen breakdown. Adrenaline did not cause any significant change in the rate of glucose load in adipocytes or in fibroblasts (Fig. 7*A*), whereas it substantially increased the rate of glucose clearance in adipocytes but only in insulin-stimulated conditions (Fig. 7*B*). Therefore, it is also possible that adrenaline, when combined with insulin, increases the glucose efflux from adipocytes. Together, these data demonstrate that although adrenaline does not alter the cytosolic glucose concentration, it has an important effect on cytosolic glucose dynamics in 3T3-L1 adipocytes.

We conclude that differentiation of 3T3-L1 fibroblasts into adipocytes leads to a progressively reduced cytosolic glucose concentration, reflecting major changes in glucose permeability and metabolism.

REFERENCES

1. Green, H., and Meuth, M. (1974) *Cell* **3,** 127–133
2. Green, H., and Kehinde, O. (1976) *Cell* **7,** 105–113
3. Whitesell, R. R., and Abumrad, N. A. (1985) *J. Biol. Chem.* **260,** 2894–2899
4. Elmendorf, J. S., and Pessin, J. E. (1999) *Exp. Cell Res.* **253,** 55–62
5. John, S. A., Ottolia, M., Weiss, J. N., and Ribalet, B. (2008) *Pflugers. Arch.* **456,** 307–322
6. Fehr, M., Lalonde, S., Lager, I., Wolff, M. W., and Frommer, W. B. (2003) *J. Biol. Chem.* **278,** 19127–19133
7. Chen, X., Cushman, S. W., Pannell, L. K., and Hess, S. (2005) *J. Proteome. Res.* **4,** 570–577
8. Trayhurn, P. (2007) *Obes. Rev.* **Suppl. 1,** 41–44
9. Poulos, S. P., Dodson, M. V., and Hausman, G. J. (2010) *Exp. Biol. Med.* (*Maywood*) **235,** 1185–1193
10. Rosen, O. M., Smith, C. J., Fung, C., and Rubin, C. S. (1978) *J. Biol. Chem.* **253,** 7579–7583
11. Resh, M. D. (1982) *J. Biol. Chem.* **257,** 6978–6986
12. James, D. E., Strube, M., and Mueckler, M. (1989) *Nature* **338,** 83–87
13. Kaestner, K. H., Christy, R. J., McLenithan, J. C., Braiterman, L. T., Cornelius, P., Pekala, P. H., and Lane, M. D. (1989) *Proc. Natl. Acad. Sci. U.S.A.* **86,** 3150–3154
14. Lafontan, M., Bousquet-Melou, A., Galitzky, J., Barbe, P., Carpéné, C., Langin, D., Berlan, M., Valet, P., Castan, I., Bouloumié, A., and Saulnier-Blache, J. S. (1995) *Obes. Res.* **3,** 507S–514S
15. Jensen, J., and Dahl, H. A. (1995) *Biochem. Mol. Biol. Int.* **35,** 145–154
16. Aslesen, R., and Jensen, J. (1998) *Am. J. Physiol.* **275,** E448–56
17. Garcia de Herreros, A., and Birnbaum, M. J. (1989) *J. Biol. Chem.* **264,** 19994–19999
18. Gruber, K., Hein, I., and von Bruchhausen, F. (1971) *Naunyn Schmiedebergs Arch. Pharmacol.* **271,** 361–373
19. Kletzien, R. F., and Perdue, J. F. (1973) *J. Biol. Chem.* **248,** 711–719
20. Purich, D. L., and Fromm, H. J. (1971) *J. Biol. Chem.* **246,** 3456–3463
21. Harrison, S. A., Buxton, J. M., and Czech, M. P. (1991) *Proc. Natl. Acad. Sci. U.S.A.* **88,** 7839–7843
22. Webb, J. L. (ed.) (1966) *Enzyme and Metabolic Inhibitors: Volume III, Iodoacetate, Maleate, N-Ethylmaleimide, Alloxan, Quinones, Arsenicals,* pp. 1–283, Academic Press, New York
23. Holman, G. D., Kozka, I. J., Clark, A. E., Flower, C. J., Saltis, J., Habberfield, A. D., Simpson, I. A., and Cushman, S. W. (1990) *J. Biol. Chem.* **265,** 18172–18179
24. Cushman, S. W., Wardzala, L. J., Hissin, P. J., Karnieli, E., Simpson, I. A., and Salans, L. B. (1983) in *The Adipocyte and Obesity: Cellular and Molecular Mechanisms* (Angel, A., Hollenberg, C. H., and Roncari, D. A., eds)

pp. 105–111, Raven Press, Ltd., New York
25. Flier, J. S. (1983) *Annu. Rev. Med.* **34,** 145–160
26. Kahn, C. R. (1978) *Metabolism* **27,** 1893–1902
27. Olefsky, J. M. (1989) in *Endocrinology* (DeGroot, L., Besser, G. M., Marshall, J. C., Nelson, D. H., Odel, W. D., Potts, J. T., Rubinstein, A. H., and Steinberger, E., ed.) pp. 1369–1388, W. B. Saunders Co., Philadelphia, PA
28. Furler, S. M., Jenkins, A. B., Storlien, L. H., Kraegen, E. W., and Barnett, D. (1991) *Am. J. Physiol.* **261,** E337–E347
29. Lefrere, I., De Coppet, P., Camelin, J. C., Le Lay, S., Mercier, N., Elshourbagy, N., Bril, A., Berrebi-Bertrand, I., Feve, B., and Krief, S. (2002) *J. Biol. Chem.* **277,** 39169–39178
30. Monjo, M., Pujol, E., and Roca, P. (2005) *Am. J. Physiol. Endocrinol. Metab.* **289,** E145–E150
31. Smith, U., Kuroda, M., and Simpson, I. A. (1984) *J. Biol. Chem.* **259,** 8758–8763
32. Joost, H. G., Weber, T. M., Cushman, S. W., and Simpson, I. A. (1986) *J. Biol. Chem.* **261,** 10033–10036
33. Joost, H. G., Weber, T. M., Cushman, S. W., and Simpson, I. A. (1987) *J. Biol. Chem.* **262,** 11261–11267
34. Mulder, A. H., Tack, C. J., Olthaar, A. J., Smits, P., Sweep, F. C., and Bosch, R. R. (2005) *Am. J. Physiol. Endocrinol. Metab.* **289,** E627–E633
35. Kuroda, M., Honnor, R. C., Cushman, S. W., Londos, C., and Simpson, I. A. (1987) *J. Biol. Chem.* **262,** 245–253
36. Nishimura, H., Saltis, J., Habberfield, A. D., Garty, N. B., Greenberg, A. S., Cushman, S. W., Londos, C., and Simpson, I. A. (1991) *Proc. Natl. Acad. Sci. U.S.A.* **88,** 11500–11504
37. Kirsch, D. M., Baumgarten, M., Deufel, T., Rinninger, F., Kemmler, W., and Häring, H. U. (1983) *Biochem. J.* **216,** 737–745